



Contents lists available at ScienceDirect

Materials Science & Engineering C

journal homepage: www.elsevier.com/locate/msec

A stimuli-responsive combination therapy for recovering p53-inactivation associated drug resistance

Leilei Guo^{a,b,c,1}, Yurui Xu^{b,c,1}, Anwei Zhou^{b,c,1}, Lei Zhang^{b,c}, Lei Sun^{b,c}, Ya Gao^{b,c}, Jianmei Chen^{b,c}, Xue Shan^{b,c}, Jikang Zhang^{b,c}, Junliang Ge^{b,c}, Xueying An^d, Xiaoxuan Liu^{a,*}, Yu Zhang^{b,c,**}, Xinghai Ning^{b,c,**}

^aState Key Laboratory of Natural Medicines and Jiangsu Key Laboratory of Drug Discovery for Metabolic Diseases, Center of Drug Discovery, Center of Advanced Pharmaceutics and Biomaterials, China Pharmaceutical University, Nanjing 210009, China

^bNational Laboratory of Solid State Microstructures, College of Engineering and Applied Sciences, Nanjing University, Nanjing 210093, China

^cChemistry and Biomedicine Innovation Center, Nanjing University, Nanjing 210093, China

^dLaboratory for Bone and Joint Diseases, Model Animal Research Center, Nanjing University, Nanjing 210093, China



ARTICLE INFO

Keywords:

Chemotherapy
Drug resistance
Tumor spheroids
MDM2 inhibitor
pH sensitive delivery systems

ABSTRACT

Drug resistance is a major hindrance in the anticancer treatment, which encourages the development of effective therapeutic strategies. For the first time, MDM2-mediated p53 degradation was identified as a critical factor for developing acquired resistance of doxorubicin (DOX) in HepG2 tumor spheroids, which could be effectively reversed by MDM2 inhibitor MI-773, thereby improving anticancer effects. Therefore, a pH-sensitive liposomal formulation of DOX and MI-773 (LipD/M@CMCS) were developed for recovering p53-mediated DOX resistance in hepatocellular carcinoma. LipD/M@CMCS were composed of cationic liposomes covered with carboxymethyl chitosan ($pI = 6.8$), and were stable in the physiological condition (pH 7.4), but rapidly converted to cationic liposomes in tumor acidic microenvironment (pH 6.5), endowing them with tumor specificity and enhanced cellular uptake. We showed that LipD/M@CMCS could not only effectively induce cell apoptosis in HepG2 tumor spheroids, but significantly inhibit tumor growth with minimal adverse effects. In summary, selective regulation of MDM2 in cancer cells is a promising strategy to overcome DOX resistance, and may provide a perspective on the management of malignant tumors.

1. Introduction

Hepatocellular carcinoma (HCC) is one of the most common malignancies, and its incidence appears rapidly increasing worldwide [1]. Although various treatments have been applied in the management of HCC [2], chemotherapy still remains the top therapeutic choice for most patients. Particularly, doxorubicin (DOX), as the first-line chemotherapeutic agent, shows effective antitumor effects on HCC, and significantly prolongs patient survival. However, its anticancer efficacy is limited due to the frequent emergence of drug resistance during the treatment [3,4]. Therefore, identifying the mechanism of drug resistance developed in tumor may provide a precise strategy for developing effective treatments aimed to fight the therapeutic resistance.

Drug resistance is an initiative and acquired protective mechanism for cancer cells to establish tolerance to pharmaceutical treatments, involving many drug-induced adaptive responses, such as drug inactivation, enhanced efflux effects, repairing DNA damage and cell death inhibition. Particularly, inherent tumor cell heterogeneity significantly affects the response of tumor cells to chemotherapy, and consequently enables drug resistance. Tumor is a complex combination of tumor cells, surrounding blood vessels, signaling molecules and the extracellular matrix, and their interactions provide a unique microenvironment, such as hypoxia, changed energy metabolism, acidic condition and cell-cycle arrest, etc. [5,6]. Therefore, the construction of a tumor cell model, which can mimic various properties of human solid tumors, can greatly promote the studies about tumor progression

*Corresponding author at: State Key Laboratory of Natural Medicines, Center of Drug Discovery, Center of Advanced Pharmaceutics and Biomaterials, China Pharmaceutical University, Nanjing 210009, China.

**Corresponding authors at: National Laboratory of Solid State Microstructures, College of Engineering and Applied Sciences, Nanjing University, Nanjing 210093, China.

E-mail addresses: xiaoxuanliucpu@163.com (X. Liu), zhangyu2016@nju.edu.cn (Y. Zhang), xning@nju.edu.cn (X. Ning).

¹ These authors made equal contributions to this work.

<https://doi.org/10.1016/j.msec.2019.110403>

Received 16 May 2019; Received in revised form 26 October 2019; Accepted 5 November 2019

Available online 06 November 2019

0928-4931/© 2019 Published by Elsevier B.V.

related biological progress, such as homeostasis, metastasis, signal transduction pathways and drug resistance [7].

Three dimensional tumor spheroids (3D tumor spheroids) are stereoscopically growing heterogeneous tumor cell populations, and possess similar properties as in vivo human solid tumors, including tumor structures, cellular constitution, gene expression, cell signal transduction, and even physiological conditions [8,9], making them an ideal tumor cell model for studying drug resistance, and especially for screening of the therapeutic candidates in early stages of the drug development [10]. Previous studies verify that 3D tumor spheroids show more resistance to chemotherapy than 2D cells mainly because of changed cell states and mutated molecular targets of drug [11,12]. To achieve compliance of this complicated situation, the combination treatment approach with multiple drugs have been utilized to increase tumor cell death while delay the emergence of drug resistance. However, current combination therapy only targets different molecular mechanisms to induce cell death, but has no effects on blocking the particular resistance mechanism developed in treatment. Consequently, it exhibits minimal effects on multiple mechanisms of resistance, and cannot resensitize drug resistant cancer cells to the original treatment, thereby limiting its therapeutic potential [13]. Therefore, effective strategies that regulate the intrinsic and acquired resistance pathway in tumors to improve treatment overcomes are urgently needed.

In this study, we have investigated the development of acquired drug resistance in 3D tumor spheroids under the long-term DOX treatment. We identified that tumor spheroids not only showed more intrinsic resistance to DOX compared to 2D cells, but gradually built up acquired drug resistance after multiple DOX challenges. Particularly, the down-regulation of p53 played a key role in acquired drug resistance, which could be overcome by MI-773, an inhibitor of MDM2, which is an important negative regulator of p53, indicating that the co-treatment of DOX and MI-773 may be a potent anticancer strategy for improving therapeutic effects, especially overcoming drug resistance. We therefore developed a pH-sensitive liposomal formulation (LipD/M@CMCS) for co-delivery of DOX and MI-773 (shown in Scheme 1), which could surmount the systemic adverse effects of DOX and poor bioavailability of MI-773 [14,15]. In comparison of traditional liposome delivery systems, stimuli-responsive nanocarriers are triggered by external and internal stimuli, allowing for selectively releasing their contents into diseased tissues. LipD/M@CMCS were designed to target tumor acidic microenvironment, and improved the synchronous uptake of DOX and MI-773 in tumor cells, thereby increasing the targeting specificity and sensitivity, overcoming drug resistance, and enhancing antitumor effects. Therefore, LipD/M@CMCS is a promising antitumor therapeutic entity that can solve fundamental issues of the drug resistance.

2. Materials and methods

2.1. Materials and instrument

Human hepatoma cell line HepG2 was obtained from the Chinese Academy of Sciences (Shanghai, China). Nude mice (6–8 weeks, 18–22 g) were purchased from Nanjing Qinglongshan Experimental Animal Center. Cell Cycle Detection Kit was purchased from BD Bioscience (New Jersey, USA). Anti-p53, anti-p21, anti-MDM2 and anti-GAPDH antibodies were purchased from Santa Cruz Bio-technologies (California, USA). Hydrogenated soy phosphatidylcholine (HSPC), 1,2-dioleoyl-3-trimethylammonium-propane (chloride salt) (DOTAP), 1,2-dioleoyl-sn-glycero-3-phosphoethanolamine (DOPE) and cholesterol were purchased from Avanti Polar Lipids (Alabaster, USA). Carboxymethyl chitosan (CMCS, average MW = 50,000 Da; degree of carboxymethyl substitution = 60%; degree of deacetylation = 85%) was purchased from Jinan Haidebei Biological Engineering Co. (Jinan, China). MI-773, RG7112 and Nutlin-3 were purchased from MedchemExpress (New Jersey, USA). Field emission SEM (Hitachi S-

4700, Tokyo, Japan) was used for characterization of tumor spheroids. Tanon-5200 (Tanon Science & Technology) was used for Chemiluminescence. The Malvern Zetasizer Nano ZS (Malvern Instruments, Malvern, UK) was used for measuring particle size and zeta potential. TEM (TEM-7650, Hitachi, Chiyoda-ku, Japan) was used for characterization of liposomes. PerkinElmer IVIS Spectrum (PerkinElmer) was used for in vivo images. All animal researches were performed in accordance with National Institute of Health Guidelines under the protocols, approved by the ethics committee at the Affiliated Drum Tower Hospital of Nanjing University Medical School.

2.2. Cell culture and 3D tumor spheroids formation

HepG2 cell was cultured in RPMI 1640 medium supplemented with 10% FBS at 37 °C in 5% CO₂. 3D tumor spheroids were constructed using the liquid-overlay 96-well approach [16]. Agarose (2%) was added into flat-bottomed 96-well plates and stored at 4 °C for 12 h, followed by adding 15,000 cells into each well. Plates were cultured in standard incubators. The 50% culture medium was exchanged every other day.

2.3. Characterization of 3D tumor spheroids using SEM

The 3D tumor spheroids were harvested and washed with ice-cold PBS 3 times. 3D tumor spheroids were fixed in 2.5% glutaraldehyde, and washed with ice-cold PBS 3 times, followed by being fixed in 1% OsO₄ in the dark. After washing with deionized water, the samples were dehydrated with gradient ethanol aqueous solution for 15 min, and dried in vacuum overnight. 3D tumor spheroids were immobilized on Conductive Copper Foil Tape and observed by field emission SEM.

2.4. Live/dead staining assay of 3D tumor spheroids

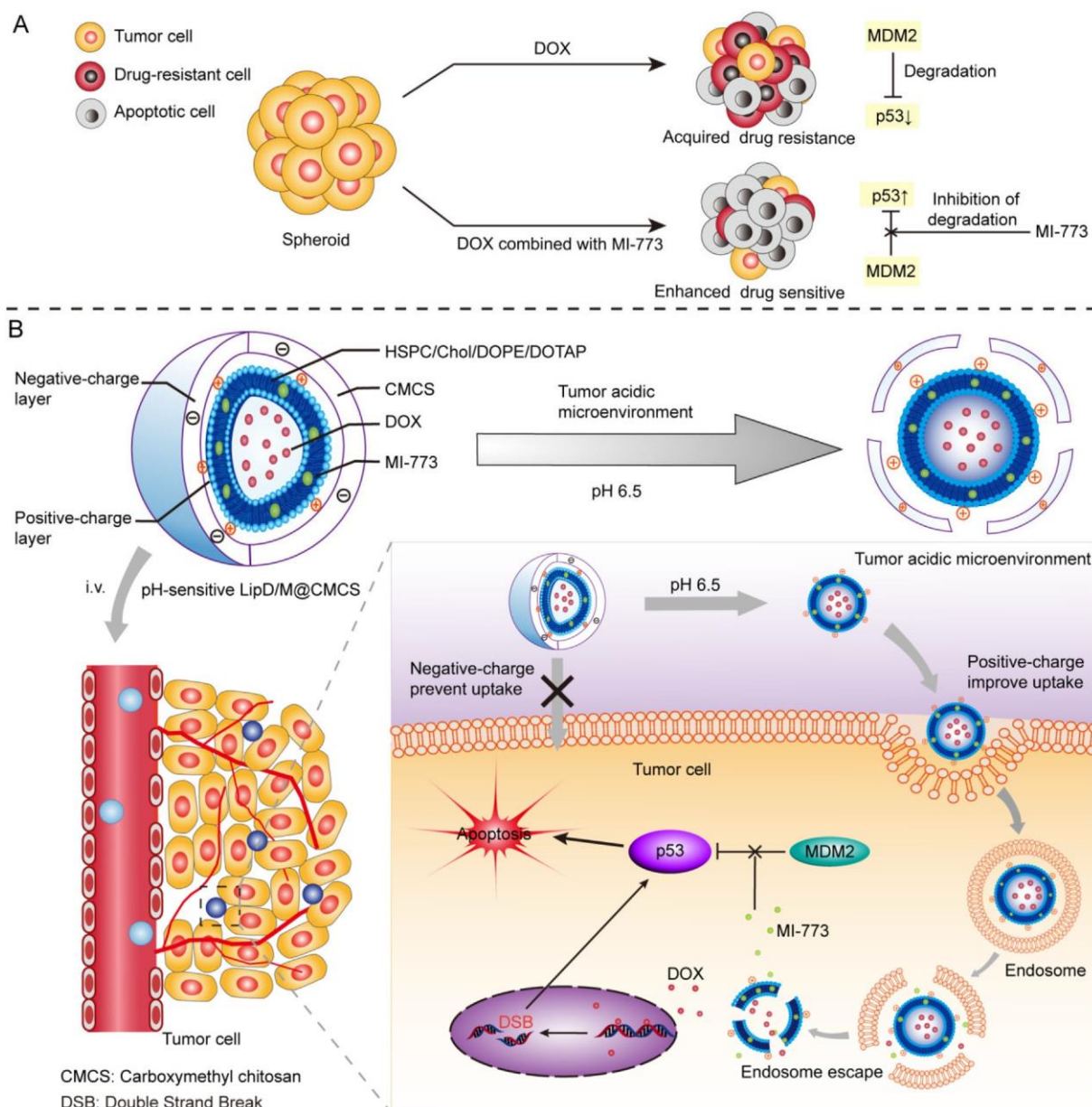
The characterization of tumor spheroids was determined using the Live/Dead staining assay [6]. The 3D tumor spheroids were washed with ice-cold phosphate-buffered saline (PBS) twice and cultured with fresh PBS containing calcein AM and propidium iodide (PI). After incubating for 30 min at 37 °C, fluorescence imaging was acquired using fluorescence microscope. Green fluorescence emission of calcein AM (Excitation: 470 nm; Emission: 525 nm) and red fluorescence (Excitation: 550 nm; Emission: 605 nm) of PI was detected.

2.5. Cell viability assays for 2D cells and 3D tumor spheroids using MTT assay

The cytotoxicity of drug against 2D cells and 3D tumor spheroids was determined by MTT assay [17]. Briefly, 2D cells and 3D tumor spheroids cultured in 96-well plates were incubated with different concentrations of drug. After corresponding incubation time, 200 μL MTT solutions was added and incubated at 37 °C. The culture medium was removed, followed by adding 150 μL of DMSO. After DMSO (100 μL) transferred to 96-well plates, the absorbance at 570 nm was read with microplate reader.

2.6. Cell viability assays for 2D cells and 3D tumor spheroids using flow cytometry

The cell viability of 2D cells and 3D tumor spheroids treated with DOX at indicating incubation time was also investigated using calcein staining followed by flow cytometry [18]. Briefly, 2D cells and 3D tumor spheroids incubated with DOX at indicating time were harvested and digested to single cells. Then, the cells were stained by calcein at 37 °C, and washed by ice-cold PBS, followed by analyzing by flow cytometry measurement measuring green fluorescence emission.



Scheme 1. (A) p53-related drug resistance in tumors can be reversed by inhibiting the interactions between MDM2 and p53. (B) pH-sensitive liposome is composed of CMCS (pI = 6.8) coating cationic liposome, which is sensitive to the tumor acidic microenvironment, and can effectively co-deliver DOX and MI-773 in cancer cells, leading to high therapeutic effects of DOX.

2.7. The uptake of DOX in 2D cells and 3D tumor spheroids

Both 2D cells and 3D tumor spheroids were incubated with DOX, and the cultured cells were harvested at different time points. The cells were digested with EDTA-trypsin into individual cells. The cells were washed with ice-cold PBS, followed by measuring with flow cytometry. At the same time, the uptake was intuitively recorded by fluorescence microscopy detected with red fluorescence of DOX.

2.8. Assessment of cell cycles

The cell cycle distribution of 2D cells and 3D spheroids were determined by flow cytometry using the Cell Cycle Detection Kit [19]. Briefly, the cells were cultured in plates for 24 h and harvested. The cells were digested with EDTA-trypsin into individual cells. Then, the cells were washed twice with ice-cold PBS, and immobilized in pre-cooled 70% ethanol overnight at 4 °C. Cells were then washed with ice-

cold PBS, and incubated with Kit solution at room temperature for 30 min, followed by analyzing by flow cytometry.

2.9. Western blot analysis

HepG2 cells were incubated with 300 μ L RIPA buffer supplemented with protease inhibitor cocktail and PMSF on the ice for 15 min, and whole proteins were extracted and quantified using BCA assay. After boiling at 95 °C for 10 min, equivalent amounts of proteins (50 μ g) were analyzed using 10% SDS polyacrylamide gel electrophoresis. Proteins were transferred onto PVDF membranes for 60 min, and were blocked with 5% skim milk for 2 h. The membranes were incubated with anti-p53, anti-p21, anti-MDM2 and anti-GAPDH antibodies at 4 °C overnight. After washing with TBST, the membranes were incubated with secondary antibody at 1:5000 dilutions for additional 2 h at room temperature, followed by detecting with the Tanon-5200 Chemiluminescence.

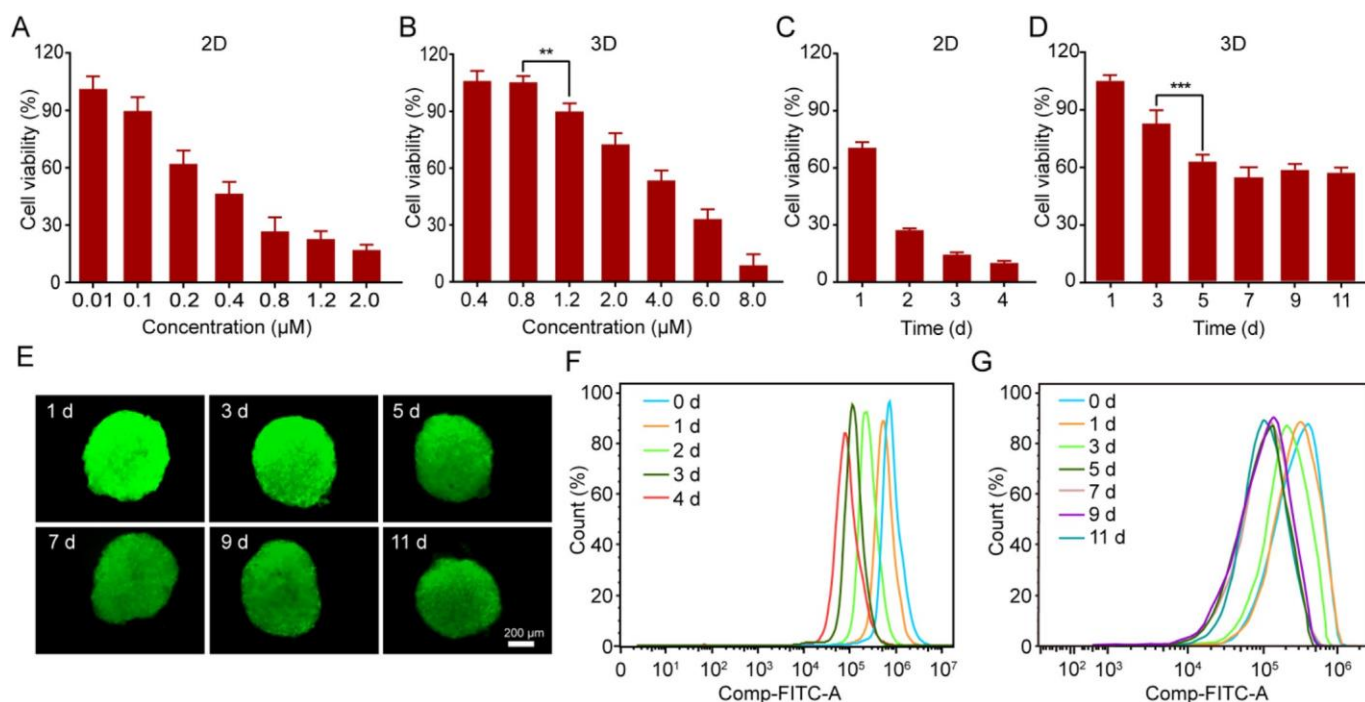


Fig. 1. Cell viability of 2D cells and 3D tumor spheroids after treatment with DOX. Cell viability of 2D cells (A) and 3D tumor spheroids (B) treated with different concentrations of DOX. Cell viability of 2D cells (C) and 3D tumor spheroids (D) treated with DOX (1.2 μM) at different time points. (E) The fluorescent images of calcein stained 3D tumor spheroids treated with DOX (1.2 μM). The scale bar represents 200 μm. Flow cytometry analyses of living cells in 2D cells (F) and 3D tumor spheroids (G) treated with DOX (1.2 μM). Values are the mean ± SD, n = 6. **, p ≤ 0.01, ***, p ≤ 0.001 as calculated by Student's t-test.

2.10. Preparation and characterization of LipD/M@CMCS

LipD/M@CMCS were prepared by thin lipid film hydration and the sequential extrusion method [20]. Briefly, HSPC, DOTAP, DOPE, cholesterol and MI-773 (80:1:1:6:9 w/w) were dissolved in chloroform and evaporated to form a thin dried film. The film was hydrated with 300 mM ammonium sulfate solution, and the liposome suspension was extruded sequentially through polycarbonate membrane filters with pore sizes of 200 and 100 nm. Free ammonium sulfate was removed by dialysis, and DOX solution was added to the liposomal suspension. The suspension was incubated for 1 h at 60 °C, and was purified by dialysis, affording cationic LipD/M, which were added into CMCS solution (2 mg/mL), generating LipD/M@CMCS. The particle size and zeta potential were measured using the Malvern Zetasizer Nano ZS. The morphology of LipD/M and LipD/M@CMCS was observed using TEM. The serum stability of LipD/M@CMCS was investigated by incubating in PBS buffer (pH 7.4) containing FBS (50% v/v) at 37 °C for 24 h.

2.11. Drug release from LipD/M@CMCS

The release of DOX and MI-773 from LipD/M@CMCS was performed using dialysis method [14]. LipD/M@CMCS solution (1.0 mL) was transferred into dialysis bags, followed by immersing into 50 mL of PBS solution containing 0.1% Tween 80 under different acidic condition (pH 7.4 and pH 6.5). The dialysis was shaken at 37 °C for 72 h, and 1.0 mL of dialysis solution was collected at different time points (2, 4, 6, 8, 10, 12, 24, 48 and 72 h). The amounts of DOX and MI-773 were determined using fluorospectrophotometer and HPLC method, respectively.

2.12. The uptake of LipD/M@CMCS in 2D cells at pH 6.5 and pH 7.4

2D cells were incubated with coumarin-6 labeled Lip@CMCS at pH 6.5 and pH 7.4 medium. Then, cells were harvested at different time points, and analyzed by flow cytometry. The fluorescence intensity of

coumarin 6 was measured using FL2 channel (Ex/Em = 466/504 nm).

2.13. In vivo biodistribution

After the nude mice were injected with DiR-labeled Lip@CMCS and DiR-labeled Lip for 24 h, nude mice were imaged in In Vivo Imager. Moreover, the tumor-bearing mice were sacrificed, and major organs were obtained and imaged.

2.14. In vivo antitumor effects of LipD/M@CMCS

The nude mice were inoculated subcutaneously with 1×10^7 HepG2 tumor cells. When the HepG2 tumor volumes reached about 100 mm³, nude mice were randomly assigned to 5 groups (n = 4) and intravenously injected with PBS, DOX (2.0 mg/kg), DOX + MI-773 (2.0 mg/kg DOX, 4.0 mg/kg MI-773), LipD@CMCS (2.0 mg/kg DOX) or LipD/M@CMCS (2.0 mg/kg DOX, 4.0 mg/kg MI-773) every three days for four weeks. Tumor volumes and body weights were measured every three days. At the end of the test, mice were sacrificed, and the tumors were collected, imaged and analyzed by TUNEL and H&E stain. The major organs, including heart, liver, spleen, lung and kidneys, were also harvested and analyzed by H&E stain.

2.15. Statistical analysis

All experiments were repeated at least 3 times. Data were expressed as mean ± SD. Statistical analyses were performed using GraphPad Prism 6 software. The differences between two groups were determined by Student's t-test. * represents p < 0.05, ** represents p < 0.01 and *** represents p < 0.001.

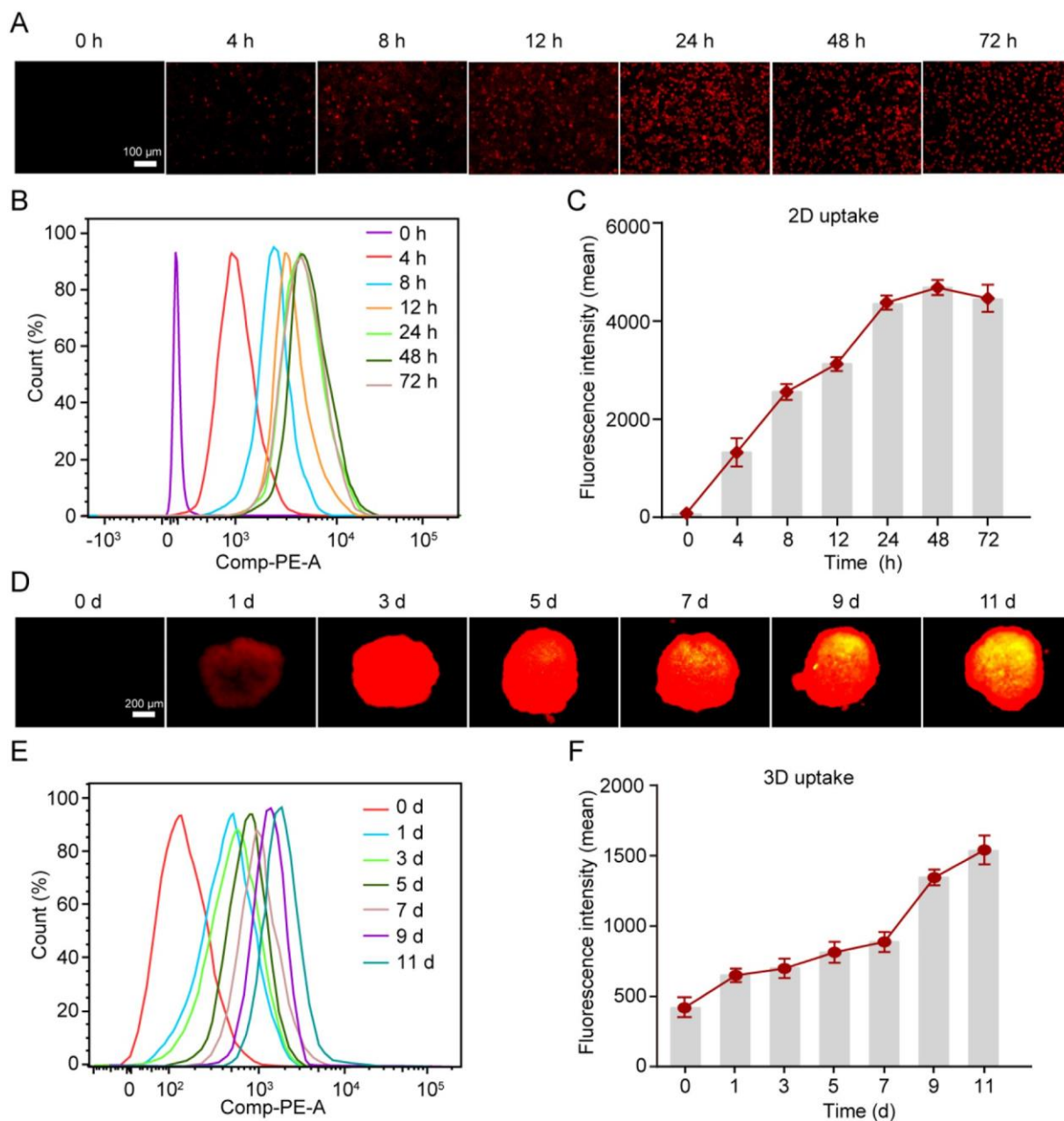


Fig. 2. The time-dependent uptake of DOX in 2D cells and 3D tumor spheroids. (A) The fluorescent images of 2D cells incubated with DOX ($1.2 \mu\text{M}$) at different time points. The scale bar represents $100 \mu\text{m}$. (B, C) Flow cytometry analyses of 2D cells incubated with DOX ($1.2 \mu\text{M}$). (D) The fluorescent images of 3D tumor spheroids incubated with DOX ($1.2 \mu\text{M}$) at different time points. The scale bar represents $200 \mu\text{m}$. (E, F) Flow cytometry analyses of 3D tumor spheroids incubated with DOX ($1.2 \mu\text{M}$). Values are the mean \pm SD, $n = 6$.

3. Results and discussion

3.1. Generation and characterization of HepG2 3D tumor spheroids

3D tumor spheroids are an important *in vitro* cell model, which possesses similar biological behaviors to the complexity and interactions present in *in vivo* tumors [21]. To successfully utilize this model to study tumor biology or screen novel therapeutic agents, it is necessary to prepare spheroids in a controlled manner. As shown in Fig. S1, HepG2 3D tumor spheroids were generated using the liquid-overlay 96-well method [16], and compact single 3D tumor spheroids about $700 \mu\text{m}$ in diameter were obtained. Fig. S2A shows that there were more necrotic cells in the interior of spheroids and more live cells in the peripheral spheroids, indicating that spheroids have similar heterogeneous cell constitution as solid tumors [9]. In addition, SEM showed

that 3D tumor spheroids had an integral spheroid morphology, and HepG2 cells kept round shapes surrounded with other cells and extracellular matrix (ECM) (Fig. S2B), allowing for mimicking morphology and microenvironment of solid tumors [22].

3.2. Evaluation of DOX sensitivity in 2D cells and 3D tumor spheroids

Cancer cells exhibit different responses to anticancer drugs in three dimensional cultures compared to monolayer cultures, and consequently generate diverse chemotherapeutic resistance. It is therefore desirable to compare the behaviors of cancer cells against treatment under 2D and 3D culture conditions. The cell viability of 2D cells and 3D tumor spheroids incubated with different concentrations of DOX was examined using MTT assay. Fig. 1A and B demonstrates that 3D tumor spheroids exhibited more resistance to DOX than 2D cells after

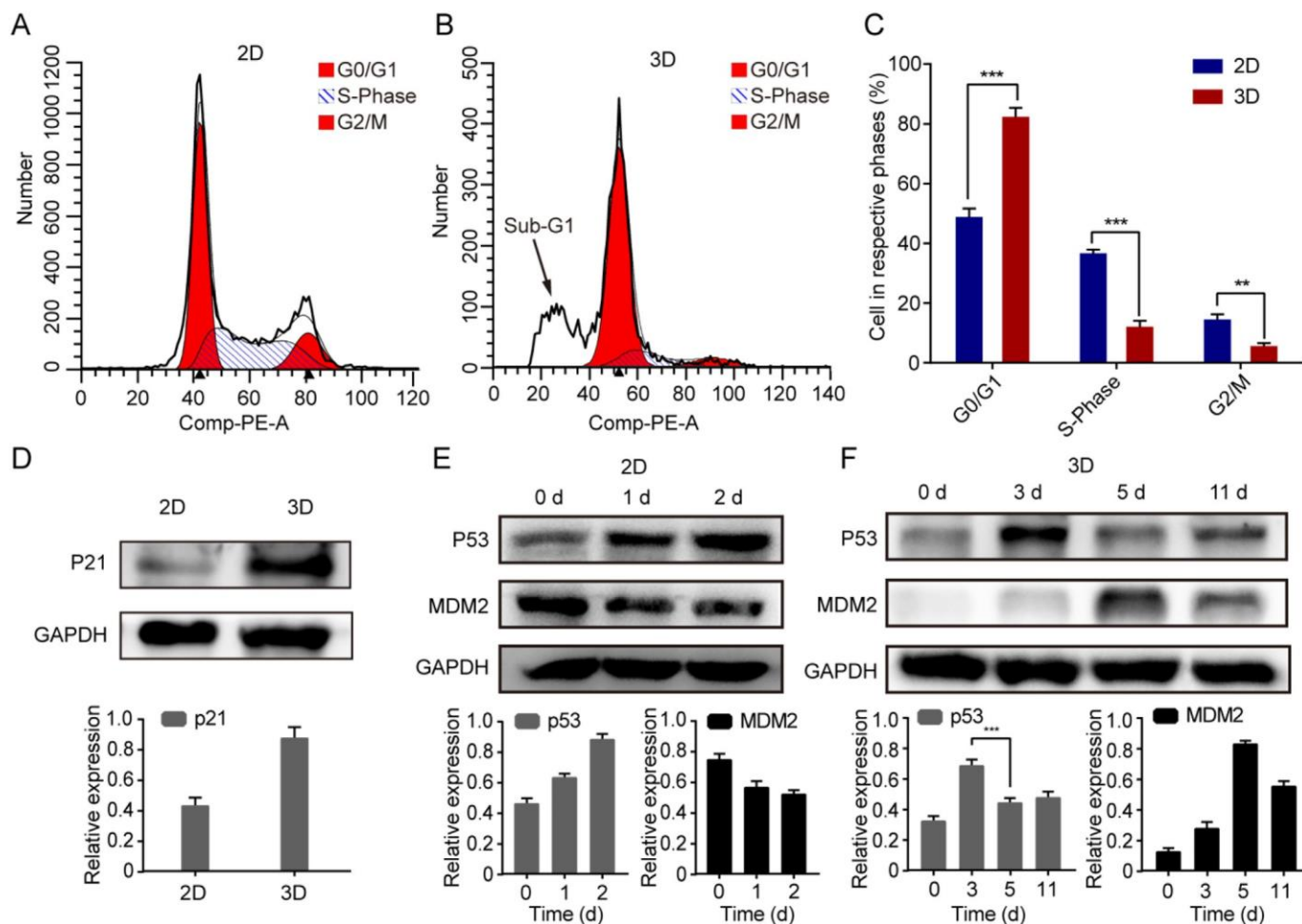


Fig. 3. The analyses of cell cycle distribution and apoptotic proteins. (A–C) The cell cycle distribution of 2D cells and 3D tumor spheroids. (D) The levels of p21 proteins in 2D cells and 3D tumor spheroids. The levels of MDM2 and p53 proteins in 2D cells (E) and 3D tumor spheroids (F) treated with DOX (1.2 μ M) at different time points. GAPDH was chosen as the reference. Values are the mean \pm SD, $n = 6$. **, $p \leq 0.01$; ***, $p \leq 0.001$ as calculated by Student's *t*-test.

48 h incubation. For example, 0.8 μ M DOX had no cytotoxic effects on 3D tumor spheroids, but induced 74% 2D cells death. Particularly, the IC_{50} of DOX in 3D tumor spheroids was 4.9 μ M, which is 12-fold higher than 2D cells (IC_{50} of 0.4 μ M), indicating low sensitivity of DOX in 3D tumor spheroids. In addition, we investigated the development of acquired drug resistance during the long-term treatment of DOX. Fig. 1C and D shows that cell viability of 3D tumor spheroids decreased to 60% after 5-day treatment, whereas no cell death was observed for additional 6-day incubation, which was further confirmed by flow cytometry (Fig. 1E–G). In contrast, the cell viability in 2D cells continuously decreased, and no DOX resistance was observed, indicating that DOX has minimal effects on solid tumors because of intrinsic drug resistance and rapid development of acquired drug resistance.

3.3. Cellular uptake of DOX in 2D cells and 3D tumor spheroids

The decrease in the cellular uptake of antitumor drugs is one of key factors for developing drug resistance [14]. We therefore investigated the uptake profiles of DOX in 3D tumor spheroids. Fig. 2 shows that DOX rapidly accumulated in 2D cells, and reached the plateau after 24 h incubation. Importantly, higher intracellular levels of DOX were observed in 2D cells compared to 3D tumor spheroids after 24 h incubation, which may contribute to high therapeutic effects on 2D cells over 3D tumor spheroids. In addition, we found that intracellular concentration of DOX in 3D tumor spheroids continuously increased during 11-day treatment, even though drug resistance appeared at

5 days, indicating that the cellular uptake of DOX is not a key factor of acquired drug resistance in 3D tumor spheroids (Fig. 2F). Therefore, low cellular uptake in 3D tumor spheroids is an important intrinsic drug resistance, which may allow for the development of acquired drug resistance during the treatment.

3.4. Cell cycle distribution in 2D cells and 3D tumor spheroids

3D tumor spheroids are composed of heterogeneous cell populations [23], and proliferative cells are located in the outer cell-layers, whereas the quiescent cells are located more centrally, leading to intrinsic resistance to chemotherapeutics [12,24]. Hence, we investigated the distribution of cell cycles in 2D cells and 3D tumor spheroids. Fig. 3A–C shows that most tumor cells (82.4%) in 3D tumor spheroids arrested at G0/G1 phase, whereas more G2/M (13.9%) and S-phase cells (37.4%) were found in 2D cells. In addition, Western blot analysis showed that 3D tumor spheroids expressed high levels of p21 protein, one significant cyclin-dependent kinase inhibitor that is associated with cellular G0/G1 phase [24], indicating the presence of more quiescent cells in 3D tumor spheroids than 2D cells (Fig. 3D). Importantly, Fig. 3B shows that an apparent amount of sub-G1 phase cells were identified in 3D tumor spheroids, indicating the presence of apoptotic and necrotic cells, which is consistent with the physiological characterization of *in vivo* human tumors (Fig. S2A). Therefore, 3D tumor spheroids possess intrinsic DOX resistance due to the presence of more quiescent cells.

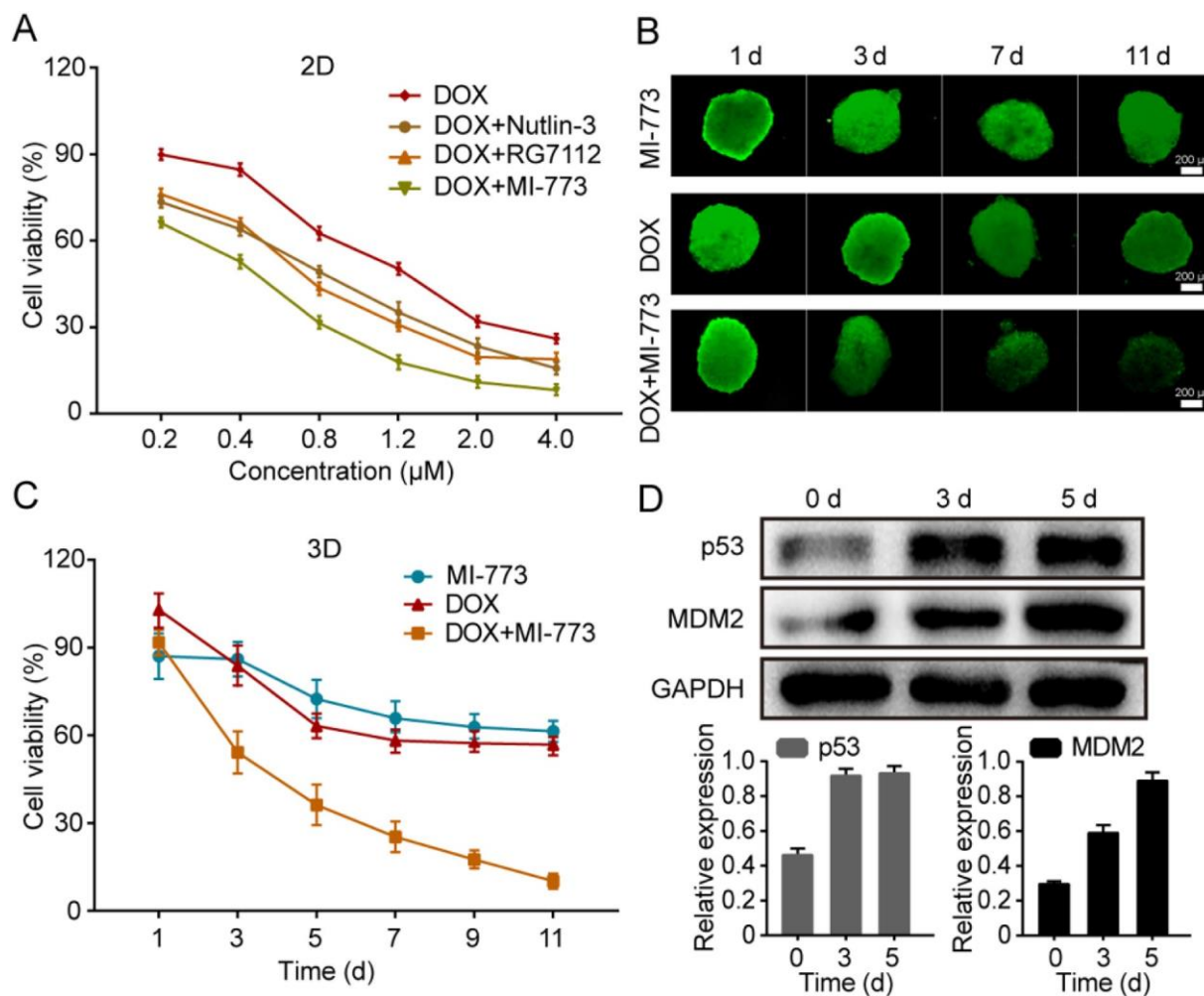


Fig. 4. The combination therapy of DOX and MDM2 inhibitor in 2D cells and 3D tumor spheroids. (A) Cell viability of 2D cells treated with different concentrations of DOX in the presence of different MDM2 inhibitors, including Nutlin-3 (3 μM), RG7112 (2.5 μM) and MI-773 (2.5 μM), by MTT assay. (B) The fluorescent images of calcein stained 3D tumor spheroids treated with MI-773 (2.5 μM), DOX (1.2 μM) or combination of DOX (1.2 μM) and MI-773 (2.5 μM) at different time points. The scale bar represents 200 μm. (C) Cell viability of 3D tumor spheroids treated with MI-773 (2.5 μM), DOX (1.2 μM) or combination of DOX (1.2 μM) and MI-773 (2.5 μM) by MTT assay. (D) The time-dependent levels of MDM2, p53 and GAPDH (reference) in 3D tumor spheroids after the 5-day co-treatment with DOX (1.2 μM) and MI-773 (2.5 μM). Values are the mean ± SD, n=6. ***, p≤0.001 as calculated by Student's t-test.

3.5. The expression of p53 in 2D cells and 3D tumor spheroids

p53 plays a key role in drug resistance through several mechanisms, including activation of DNA repair proteins, induction of cell cycle arrest at G1/S regulation point and initiation of programmed cell death [25,26]. Particularly, p53 levels in cancer cells are closely associated with antitumor effects of DOX [27], we therefore investigated the expression of p53 in 3D tumor spheroids under the DOX treatment. Fig. 3F shows that the increase in p53 levels, accompanied with cell apoptosis, was observed in 3D tumor spheroids during the first 3-day treatment. While, the long-term DOX incubation decreased p53 levels, which is consistent with the development of acquired drug resistance in 3D tumor spheroids (Fig. 1D). In contrast, 2D cells continually expressed p53 without emerging drug resistance, and more than 90% cancer cells were eventually killed after 4-day treatment (Fig. 3E). In addition, we also measured the levels of MDM2, which negatively regulates p53 through ubiquitin-mediated proteolysis [28]. Fig. 3E and F shows that the expressions of MDM2 were corresponded to the changes of p53 in 2D cells and 3D tumor spheroids. In comparison of decreased MDM2 levels in 2D cells under the DOX treatment, a significant increase in MDM2 levels was found in 3D tumor spheroids, and kept maintaining at high levels during treatment. Therefore, MDM2 mediated decline of

p53 in 3D tumor spheroids is a key factor for the initiation of the acquired drug resistance, indicating that MDM2 regulation is a promising strategy for recovering drug resistance.

3.6. Combination treatment of MDM2 inhibitor and DOX

MDM2 has been recognized as a critical molecular target for the management of tumor [29]. The pharmacological targeting of MDM2 to increase p53 expression and activity represents a promising strategy for tumor therapy [30]. A series of MDM2 inhibitors have been developed and reported to target the P53-MDM2/X axis [31]. Therefore, we investigated and compared the ability of different MDM2 inhibitors to improve anticancer effects of DOX in HepG2 cells using MTT assay. Fig. 4A reveals that co-treatment of different concentrations of DOX (0.2–4.0 μM) and MDM2 inhibitors at a concentration of IC₅₀, including Nutlin-3 (3 μM), RG7112 (2.5 μM) or MI-773 (2.5 μM), could promote cytotoxicity in comparison of DOX alone. Particularly, MI-773 displayed higher combinational effects with DOX than Nutlin-3 and RG7112, indicating that the combination therapy of DOX and MI-773 is a promising anticancer therapeutics for overcoming drug tolerance. In addition, co-treatment of DOX at a concentration more than 1.2 μM with MI-773 (2.5 μM) exhibited the best combinational anticancer

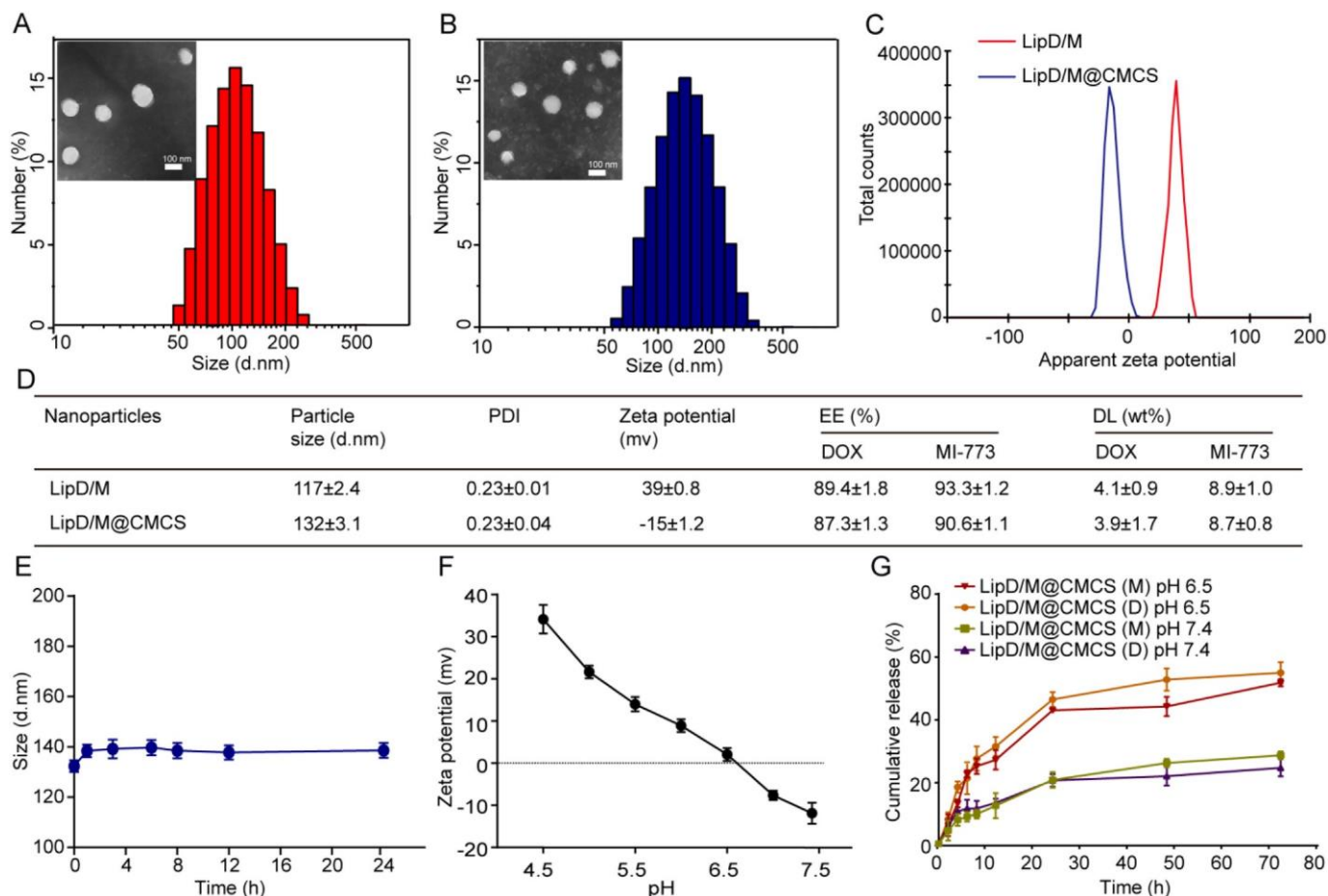


Fig. 5. Preparation and characterization of LipD/M@CMCS. TEM images and size distributions of LipD/M (A) and LipD/M@CMCS (B). The scale bar represents 100 nm. (C) Zeta potential of LipD/M and LipD/M@CMCS. (D) Sizes, polydispersity index (PDI), zeta potential, encapsulation efficiency (EE) and drug loading rates (DL) of LipD/M and LipD/M@CMCS. (E) Stability of LipD/M@CMCS in PBS buffer containing FBS (50% v/v). (F) Zeta potential of LipD/M@CMCS at various pH. (G) In vitro drug release of LipD/M@CMCS in PBS at pH 6.5 and 7.4. Values are the mean \pm SD, n = 6.

effects. We also calculate the combination index (CI) of co-treatment of DOX and MI-773 according to IC_{50} value by using Calcsyn 2.0 with 0.6533 (Table S1), indicating enhanced synergistic effect of DOX and MI-773 (CI < 1 indicates synergism).

To further investigate if the co-treatment of DOX and MI-773 could prevent the development of drug resistance in 3D tumor spheroids, we performed experiments to evaluate a combination therapy of DOX and MI-773 in 3D tumor spheroids. Fig. 4B and C shows that co-treatment can induce more than 90% cell death in tumor 3D tumor spheroids, and whereas, either DOX or MI-773 had limited impacts on their cell viability, indicating that MI-773 can recover DOX resistance. Meanwhile, Fig. 4D shows that co-treatment of DOX and MI-773 could increase both levels of p53 and MDM2 in 3D tumor spheroids during 5-day treatment. For example, the levels of p53 quickly reached plateau, and did not decrease when MDM2 gradually increased. Therefore, combination therapy of DOX and MI-773 is a promising anticancer strategy to overcoming drug resistance by inhibiting MDM2 functions.

3.7. Preparation and characterization of pH-sensitive LipD/M@CMCS

For co-treatment of DOX and MI-773, it is difficult to achieve synergistic effect in vivo due to systemic adverse effects of DOX and poor bioavailability of MI-773 [14,15]. Liposomes are bilayer microscopic vesicles, and can effectively deliver both hydrophilic and hydrophobic drugs [32], making it an ideal deliver system for combination therapy. Thus, we have developed a pH-sensitive charge-conversional liposomal formulation of DOX and MI-773 (LipD/M@CMCS) (Scheme 1). LipD/

M@CMCS are composed of cationic liposome covered with CMCS (pI = 6.8), which improves biocompatibility, prolongs systemic circulation, and increases tumor specificity by targeting tumor acidic microenvironment. As shown in Fig. 5A–D, DLS and TEM demonstrated that LipD/M@CMCS had uniform spherical morphology with average sizes of 130 nm and zeta potential of -15 mV. In addition, Fig. 5E shows that LipD/M@CMCS had good serum stability, indicating that they are optimal nano-carriers for in vivo applications. Moreover, we also investigated their ability to reverse surface potentials in response to acidic conditions. Fig. 5C shows that LipD/M and LipD/M@CMCS had zeta potential of $+39$ mV, -15 mV at pH 7.4, respectively, suggesting CMCS coating of cationic LipD/M. Whereas, LipD/M@CMCS rapidly changed to positively charged liposomes at pH 6.5 (Fig. 5F), which can enhance cellular uptake and endosomal escape [33], indicating their acidic sensitive profiles. LipD/M@CMCS were stable in the physiological condition (pH 7.4), but rapidly disintegrated in tumor acidic microenvironment (pH 6.5) to release cationic LipD/M, endowing them with tumor specificity. Furthermore, the drug release studies of LipD/M@CMCS also confirmed their pH responsiveness. Fig. 5G shows that LipD/M@CMCS exhibited slow release of DOX and MI-773 at pH 7.4, and only 16% drugs were released within 12 h, suggesting that LipD/M@CMCS have good biostability and are suitable for in vivo applications. In the contrast, DOX and MI-773 were quickly released from LipD/M@CMCS at pH 6.5, indicating that LipD/M@CMCS have excellent tumor targeting and controlled release properties.

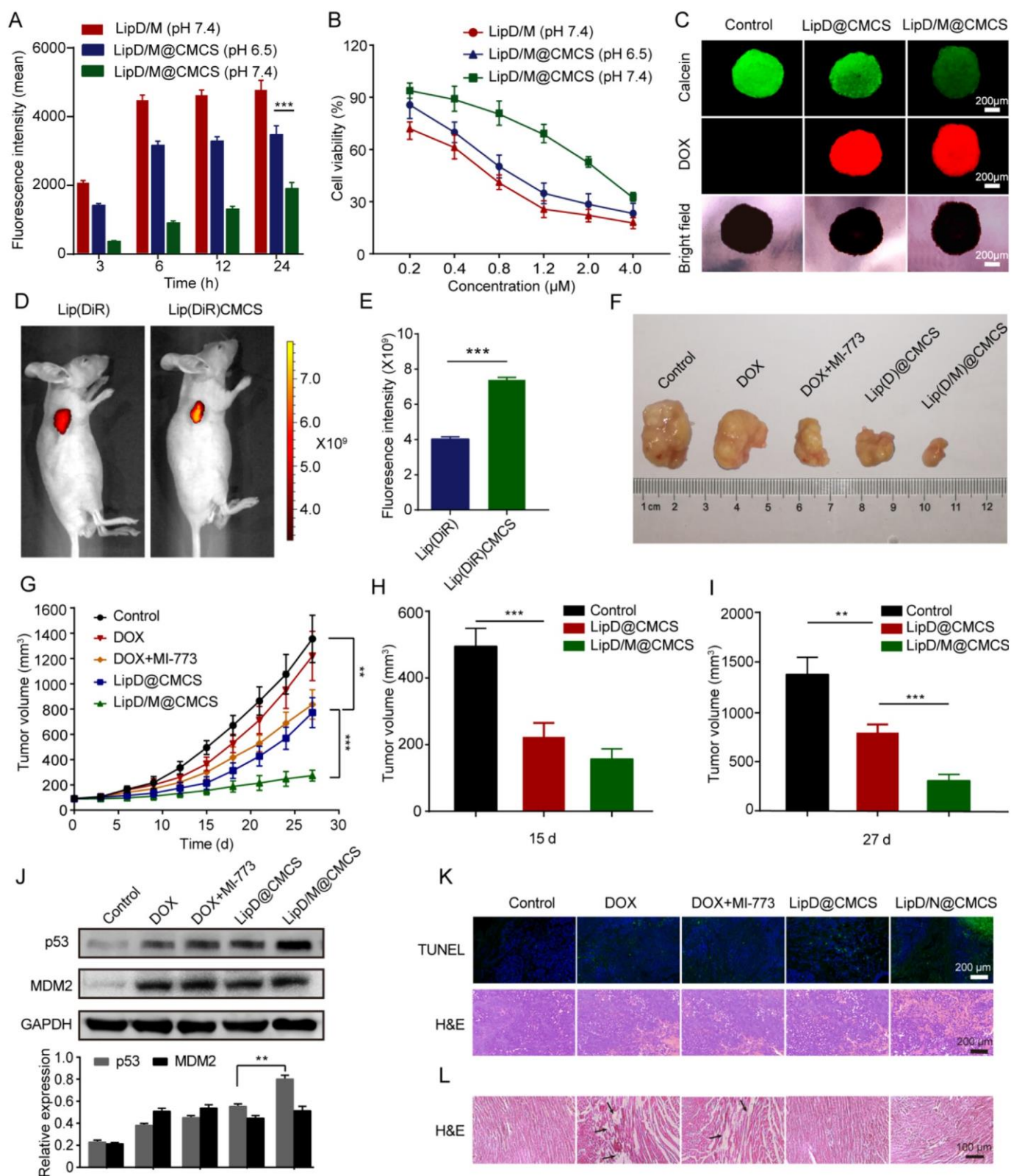


Fig. 6. In vitro and in vivo applications of LipD/M@CMCS. (A) The cellular uptake of LipD/M@CMCS in 2D cells at pH 6.5 and 7.4. (B) The cytotoxicity of LipD/M@CMCS in 2D cells at pH 6.5 and 7.4 after 24 h incubation. (C) The uptake and cytotoxicity of LipD@CMCS and LipD/M@CMCS in 3D tumor spheroids after 9 d incubation. Green fluorescence represents Calcein. Red fluorescence represents DOX. The scale bar represents 200 μm. (D) The tumor accumulation of LipDiR@CMCS in HepG2 tumor xenograft mice after 24 h administration. (E) The mean fluorescence intensities of LipDiR@CMCS after 24 h administration. (F) Images of isolated tumors at the end of the treatment. (G) Tumor growth profiles in nude mice treated with PBS, DOX, DOX + MI-773, LipD@CMCS or LipD/M@CMCS. (H) Tumor volumes after 15-day treatment. (I) Tumor volumes after 27-day treatment. (J) The relative p53 levels in isolated tumor tissues. (K) TUNEL and H&E stains of tumor slices. The scale bar represents 200 μm. (L) Histopathological analyses of heart tissues treated with PBS, DOX, DOX + MI-773, LipD@CMCS or LipD/M@CMCS. The scale bar represents 100 μm. Values are the mean ± SD, n = 4. *, p ≤ 0.05; **, p ≤ 0.01, ***, p ≤ 0.001 as calculated by Student's t-test. (For interpretation of the references to color in this figure legend, the reader is referred to the web version of this article.)

3.8. Anticancer effects of LipD/M@CMCS in vitro

LipD/M@CMCS were composed of cationic liposome covered by CMCS ($pI = 6.8$), which could effectively inhibit the cellular uptake due to negatively charged surface. However, CMCS converted to positive polyelectrolytes in acidic tumor microenvironment ($pH \sim 6.5$) and detached from cationic liposomes, consequently improving their cellular transport [34]. We therefore investigated the cellular uptake of LipD/M@CMCS at $pH 6.5$ and 7.4 . Fig. 6A shows that LipD/M@CMCS had low cellular uptake at $pH 7.4$, and whereas, displayed high DOX accumulation in cancer cells at $pH 6.5$, which is similar with cationic LipD/M, indicating that LipD/M@CMCS has good tumor targeting profiles. In addition, we performed MTT assay to confirm pH-responsive anticancer effects of LipD/M@CMCS. Fig. 6B shows that LipD/M@CMCS displayed different anticancer effects at $pH 7.4$ and 6.5 with IC_{50} of $2.5 \mu M$ and $0.9 \mu M$, respectively. For example, LipD/M@CMCS, containing $1.2 \mu M$ DOX and $2.5 \mu M$ MI-773, induced 60% cell death at $pH 6.5$, and whereas only 30% cell death was detected at $pH 7.4$, indicating that LipD/M@CMCS can significantly reduce cytotoxicity to healthy tissues. To further investigate the synergistic action of DOX and MI-773 for recovering drug resistance, we utilized 3D tumor spheroids model to test antitumor effects of LipD/M@CMCS in vitro. As shown in Fig. 6C, LipD/M@CMCS induced more cellular death compared to LipD@CMCS without MI-773, even though they had similar cellular uptake of DOX, suggesting that LipD/M@CMCS can sensitize cancer cells to DOX in tumors.

3.9. Antitumor efficacy of LipD/M@CMCS in vivo

Tumor specific drug delivery systems have demonstrated the potential to improve treatment efficacy and avoid toxicity in normal cells due to features such as high selective accumulation in tumors and active cellular uptake [35]. LipD/M@CMCS were designed to target tumor acidic microenvironment, and had an ability to improve tumor specificity of co-treatment of DOX and MI-773. We therefore performed tumor targeting studies to identify accumulation of LipD/M@CMCS in tumors. Fig. 6D and E shows that DiR-labeled Lip@CMCS (Lip-DiR@CMCS) selectively accumulated in tumors after 24 h administration, in comparison of DiR-labeled cationic liposomes (LipDiR), indicating that pH-responsive CMCS can reduce non-specific binding during circulation, and selectively release cationic liposomes in tumor acidic microenvironment, consequently enhancing cancer cellular uptake. In addition, biodistribution studies further confirmed the tumor specificity of Lip@CMCS (Fig. S4).

We further evaluated their antitumor efficacy of LipD/M@CMCS in HepG2 tumor xenograft models. As shown in Fig. 6F and G, intravenous administration of free DOX with MI-773, or LipD@CMCS only moderately retarded the tumor growth, whereas LipD/M@CMCS significantly induced cell apoptosis and death in tumors, which was further confirmed by TUNEL and H&E stain (Fig. 6K and L). Although co-treatment of free DOX and MI-773 displayed effective anticancer effects on HepG2 cells in vitro, it could not inhibit tumor growth in vivo, indicating that liposome-based combination therapy can improve synergistic effects of DOX and MI-773. More importantly, LipD@CMCS could only inhibit tumor growth during the first 15-day treatment, and tumor restart growing under additional 12-day treatment due to rapid development of acquired DOX resistance (Fig. 6H and I). In contrast, no tumor progression was detected during 27-day therapy of LipD/M@CMCS, suggesting co-treatment of DOX and MI-773 can improve long-term antitumor effects. In addition, Western blot analysis further confirmed that LipD/M@CMCS could increase p53 levels in tumors, and consequently prevent the development of acquired drug resistance (Fig. 6J). Furthermore, LipD/M@CMCS showed good biocompatibility, and no changes in behaviors and body weights and tissue damages were observed (Figs. S5 and S6), in comparison of free DOX with/without MI-773 (Fig. 6L), indicating that LipD/M@CMCS are an effective long-term

DOX treatment without systemic adverse effects.

4. Conclusion

In this work, we have identified that HepG2 tumor spheroids rapidly develop acquired drug resistance during DOX treatment by down-regulating p53, which could be recovered by co-treatment with MDM2 inhibitor MI-773, for the first time. We therefore developed a pH-sensitive liposomal formulation of DOX and MI-773 (LipD/M@CMCS) for overcoming acquired DOX resistance. LipD/M@CMCS converted to cationic liposomes in acidic tumor microenvironment, thereby endowing them with tumor specificity and improved cellular uptake. Particularly, in vivo antitumor studies showed that LipD/M@CMCS improved therapeutic efficacy, overcame drug resistance and reduced systemic toxicity, in comparison of free DOX with MI-773 and LipD@CMCS. Given these encouraging results, stimuli responsive combination therapy of DOX and MI-773 represents a potent therapeutic strategy for the management of malignant tumors.

Declaration of competing interest

The authors declare that they have no known competing financial interests or personal relationships that could have appeared to influence the work reported in this paper.

Acknowledgements

This work was supported by the The National Key Research and Development Program of China (Grant No. 2018YFB1105400), The National Natural Science Foundation of China (Grant No. 21708019, 51773227, 81701815), The Natural Science Foundation of Jiangsu Province (Grant No. BK20180334, BK20170735), the Six Talent Peaks Project in Jiangsu Province of China, the State Key Laboratory of Natural Medicines at China Pharmaceutical University (Grant No. SKLNMKF201703, SKLNMZZRC201804), the Jiangsu Specially-Appointed Professors Program, The Thousand Talents Program for Young Researchers, Fundamental Research Funds for Central Universities, The Shuangchuang Program of Jiangsu Province, The Fundamental Research Funds for Central Universities Nanjing University, The Scientific Research Foundation of Graduate School of Nanjing University (Grant No. 2017ZDL04) The Key Research and Development Program of Jiangsu Provincial Department of Science and Technology of China (Nos. BE2019002)..

Appendix A. Supplementary data

Supplementary data to this article can be found online at <https://doi.org/10.1016/j.msec.2019.110403>.

References

- [1] P. Bertuccio, F. Turati, G. Carioli, T. Rodriguez, C. La Vecchia, M. Malvezzi, E. Negri, *J. Hepatol.* 67 (2017) 302–309.
- [2] D. Zhang, A. Zheng, J. Li, M. Wu, Z. Cai, L. Wu, Z. Wei, H. Yang, X. Liu, J. Liu, *Adv. Sci.* 4 (2017) 1600460.
- [3] C. Holohan, S.V. Schaeysbroeck, D.B. Longley, P.G. Johnston, *Nat. Rev. Cancer* 13 (2013) 714–726.
- [4] R. Ruizgonzález, P. Milán, R. Bresolíobach, J. Stockert, A. Villanueva, M. Cañete, S. Nonell, *Cancers* 9 (2017) 18.
- [5] L.A. Liotta, E.C. Kohn, *Nature* 411 (2001) 375–379.
- [6] T. Wu, Y. Dai, *Cancer Lett.* 387 (2017) 61–68.
- [7] W. Asghar, R.E. Assal, H. Shafiee, S. Pitteri, R. Paulmurugan, U. Demirci, *Mater. Today* 18 (2015) 539–553.
- [8] E. Fennema, N. Rivron, J. Rouwkema, C.V. Blitterswijk, J.D. Boer, *Trends Biotechnol.* 31 (2013) 108–115.
- [9] S. Nath, G.R. Devi, *Pharmacol. Ther.* 163 (2016) 94–108.
- [10] M. Ravi, A. Ramesh, A. Pattabhi, *J. Cell. Physiol.* 232 (2017) 2679–2697.
- [11] G. Housman, S. Byler, S. Heerboth, K. Lapinska, M. Longacre, N. Snyder, S. Sarkar, *Cancers* 6 (2014) 1769–1792.
- [12] K.A. Beaumont, D.S. Hill, S.M. Daignault, G.Y. Lui, D.M. Sharp, B. Gabrielli,

- W. Weninger, N.K. Haass, J. Investig. Dermatol. 136 (2016) 1479–1489.
- [13] C. Bai, M. Yang, Z. Fan, S. Li, T. Gao, Z. Fang, J. Exp. Clin. Cancer Res. 34 (2015) 58–68.
- [14] T. Wei, C. Chen, J. Liu, C. Liu, P. Posocco, X. Liu, Q. Cheng, S. Huo, Z. Liang, M. Fermeglia, S. Pricl, X.J. Liang, P. Rocchi, L. Peng, Proc. Natl. Acad. Sci. U. S. A. 112 (2015) 2978–2983.
- [15] J. Lu, S. Guan, Y. Zhao, Y. Yu, Y. Wang, Y. Shi, X. Mao, K.L. Yang, W. Sun, X. Xu, Oncotarget 7 (2016) 82757–82769.
- [16] J. Friedrich, C. Seidel, R. Ebner, L.A. Kunz-Schughart, Nat. Protoc. 4 (2009) 309–324.
- [17] J. Li, Y. Zhou, W. Chen, Z. Yuan, B. You, Y. Liu, S. Yang, F. Li, C. Qu, X. Zhang, ACS Appl. Mater. Interfaces 10 (2018) 36641–36651.
- [18] H. Ma, Q. Jiang, S. Han, Y. Wu, J.C. Tomshine, D. Wang, Y. Gan, G. Zou, X.-J. Liang, Mol. Imaging 11 (2012) 487–498.
- [19] Y. Ma, Y. Zhu, C. Wang, D. Pan, S. Liu, M. Yang, Z. Xiao, X. Yang, W. Zhao, X. Zhou, Biomaterials 178 (2018) 147–157.
- [20] P. Guo, J. Huang, Y. Zhao, C.R. Martin, R.N. Zare, M.A. Moses, Small 14 (2018) 1703493.
- [21] W. Metzger, S. Rother, T. Pohlemann, S. Möller, M. Schnabelrauch, V. Hintze, D. Scharnweber, Mater. Sci. Eng. C 73 (2017) 310–318.
- [22] X. Xu, M.C. Farach-Carson, X. Jia, Biotechnol. Adv. 32 (2014) 1256–1268.
- [23] M. Chatziniokolaidou, Drug Discov. Today 21 (2016) 1553–1560.
- [24] M.A. Shah, G.K. Schwartz, Clin. Cancer Res. 7 (2001) 2168–2181.
- [25] T. Stiewe, T.E. Haran, Drug Resist. Updat. 38 (2018) 27–43.
- [26] Y. Shetzer, H. Solomon, G. Koifman, A. Molchadsky, S. Horesch, V. Rotter, Carcinogenesis 35 (2014) 1196–1208.
- [27] J. Cox, S. Weinman, Hepatic Oncol. 3 (2016) 57–59.
- [28] B. Vogelstein, D. Lane, A.J. Levine, Nature 408 (2000) 307–310.
- [29] A. Burgess, K.M. Chia, S. Haupt, D. Thomas, Y. Haupt, E. Lim, Front. Oncol. 6 (2016).
- [30] S.J. Kim, M. Akita, Y.N. Sung, K. Fujikura, J.H. Lee, S. Hwang, E. Yu, K. Otani, S.M. Hong, Y. Zen, Am. J. Surg. Pathol. 42 (2018) 1–11.
- [31] V. Tisato, R. Voltan, A. Gonelli, P. Secchiero, G. Zauli, J. Hematol. Oncol. 10 (2017) 133–150.
- [32] L. Feng, L. Cheng, Z. Dong, D. Tao, T.E. Barnhart, W. Cai, M. Chen, Z. Liu, ACS Nano 11 (2016) 927–937.
- [33] Y. Obata, S. Tajima, S. Takeoka, J. Control. Release 142 (2010) 267–276.
- [34] T. Mizuhara, K. Saha, D.F. Moyano, C.S. Kim, B. Yan, Y.K. Kim, V.M. Rotello, Angew. Chem. 54 (2015) 6567–6570.
- [35] M. Mathiyazhakan, C. Wiraja, C. Xu, Nano-Micro Lett. 10 (2018) 10.